

PAPER • OPEN ACCESS

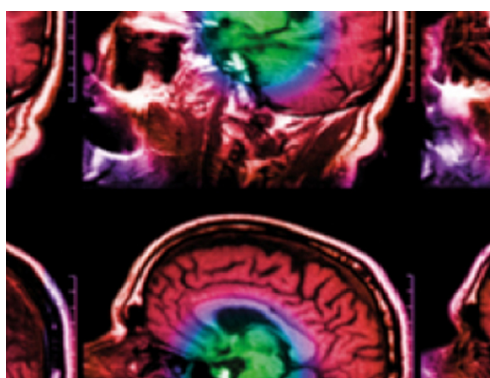
A 4D flow cardiovascular magnetic resonance study of flow asymmetry and haemodynamic quantity correlations in the pulmonary artery

To cite this article: Henrike Gbinigie *et al* 2021 *Physiol. Meas.* **42** 025005

View the [article online](#) for updates and enhancements.

You may also like

- [Enhancement of ORR Activity and Durability of Pt Single Crystal Electrodes Modified with Alkylamines](#)
Keiichiro Saikawa, Masashi Nakamura and Nagahiro Hoshi
- [Black holes, gravitational waves and fundamental physics: a roadmap](#)
Abbas Askar, Chris Belczynski, Gianfranco Bertone et al.
- [2021 roadmap on lithium sulfur batteries](#)
James B Robinson, Kai Xi, R Vasant Kumar et al.



IPEM | IOP

Series in Physics and Engineering in Medicine and Biology

Your publishing choice in medical physics,
biomedical engineering and related subjects.

Start exploring the collection—download the
first chapter of every title for free.



PAPER

A 4D flow cardiovascular magnetic resonance study of flow asymmetry and haemodynamic quantity correlations in the pulmonary artery

OPEN ACCESS

RECEIVED
27 July 2020REVISED
15 December 2020ACCEPTED FOR PUBLICATION
22 January 2021PUBLISHED
5 March 2021

Original content from this work may be used under the terms of the [Creative Commons Attribution 4.0 licence](#).

Any further distribution of this work must maintain attribution to the author(s) and the title of the work, journal citation and DOI.

Henrike Gbinigie¹, Louise Coats^{2,3}, Jehill D Parikh⁴, Kieren G Hollingsworth⁴ and Lian Gan¹ ¹ Department of Engineering, Durham University, Durham, DH1 3LE, United Kingdom² Population Health Sciences Institute, Newcastle University, Newcastle upon Tyne, NE1 3BZ, United Kingdom³ Adult Congenital and Paediatric Heart Unit, Freeman Hospital, Newcastle upon Tyne Hospitals NHS Foundation Trust, NE7 7DN, United Kingdom⁴ Newcastle Magnetic Resonance Centre, Translational and Clinical Research Institute, Newcastle University, Newcastle upon Tyne, NE4 5PL, United KingdomE-mail: lian.gan@durham.ac.uk**Keywords:** flow asymmetry, pulmonary artery, 4D flow MRISupplementary material for this article is available [online](#)

Abstract

Objective. In this paper we elucidate the asymmetric flow pattern and the haemodynamic quantity distributions and correlations in the pulmonary artery (PA) vasculature in healthy adults having structurally normal hearts, to provide reference on the flow characteristics in the PA and the right ventricle. **Approach.** Velocity data are acquired non-invasively from 18 healthy volunteers by 4D flow magnetic resonance imaging, resolved to 20 phases with spatial resolution $3 \times 3 \times 3 \text{ mm}^3$. Interpolation is applied to improve the accuracy in quantifying haemodynamic quantities including kinetic energy, rotational energy, helicity and energy dissipation rate. These quantities are volumetrically normalised to remove size dependency, representing densities or local intensity. **Main results.** Flow asymmetry in the PA is quantified in terms of all the flow dynamic quantities and their correlations. The right PA has larger diameter and higher peak stroke velocity than the left PA. It also has the highest rotational energy intensity. Counter-rotating helical streams in the main PA appear to be associated with the unidirectional helical flow noticed in the left and the right PA near the peak systole. **Significance.** This study provides a fundamental basis of normal flow in the PA. It implies the validity to use these flow pattern-related quantitative measures to aid with the identification of abnormal PA flow non-invasively, specifically for detecting abnormalities in the pulmonary circulation and response to therapy, where haemodynamic flow is commonly characterised by increased vortical and helical formations.

1. Introduction

The knowledge of flow patterns and haemodynamic quantitative metrics in the pulmonary artery (PA) and the connection with those of the right ventricle (RV) in the structurally normal heart is relatively limited but has potential significance in the pathology of some right heart related cardiovascular diseases. The right heart has traditionally been considered less significant in the whole heart function and has remained understudied in comparison to the left heart. Recognition of the need for deeper understanding of the RV function arrived only relatively recently, with the identification of its function and failure as the chief prognostic marker of survival in various forms of diseases in the pulmonary circulation, e.g. pulmonary hypertension (PH) (Sztrymf *et al* 2010, Lahm *et al* 2018), which results in high morbidity despite advances in the treatment of the disease, often due to the delayed diagnosis and/or misdiagnosis. At present clinically relevant and reliable haemodynamic quantities in the right heart are usually obtained by the highly invasive right heart catheterization. It underpins the drive for

further non-invasive quantitative markers to be implemented in the PA, which carry less risk and could be performed regularly (Schäfer *et al* 2017).

RV dysfunction is also a key feature in various types of congenital heart disease such as tetralogy of Fallot, transposition of the great arteries repaired with atrial switch, Ebstein anomaly and Eisenmenger syndrome (Diller *et al* 2007). This led to increased importance being placed on the right heart function and RV-pulmonary circulation, since the function of the RV is directly reflected in the pulmonary flow given their mechanical coupling (Vildbrad *et al* 2015, Braun *et al* 2018, Hur and Sugeng 2019). Distorted haemodynamic flow pattern is also associated with the surgical repair of congenital heart disease, due to the deviation of the PA from its normal morphology such as in the repair of the transposition of great arteries when the Lecompte manoeuvre is performed (Capuano *et al* 2019). A comprehensive understanding of what happens in healthy subjects is therefore crucial.

Non-invasive imaging of cardiovascular haemodynamic flow has the potential of improving the prognosis of the RV-related diseases, by accelerating diagnosis and treatment (Hur and Sugeng 2019). 4D flow magnetic resonance imaging (MRI) is a non-invasive and quantitative imaging tool that pairs 3D images with encoded velocity data in all 3 directions and is also time-resolved (the 4th dimension). The data is captured over the cardiac cycle for each voxel in the region of interest being imaged in a 'phase-averaged' manner (Kilner *et al* 2000). The evolution of 4D flow MRI has enabled comprehensive understanding of blood flow in the heart and great vessels such as the PA and aorta (Firmin *et al* 1993, Markl *et al* 2011, Schäfer *et al* 2017). In recent years, advances in the acquisition and post-processing of 4D flow MRI, combined with computational fluid dynamics has contributed to a deeper insight into normal and abnormal cardiac physiology and is now an established technique employed in the research setting (van der Geest and Garg 2016).

Visualisation of flow patterns and quantitative analyses of kinetic energy (KE), vorticity, wall shear stress and mean flow in the PA were realised by 4D flow MRI in a number of studies recently. Reiter *et al* (2008) found the existence of a vortical structure in the main pulmonary artery (MPA) along the orientation of the right ventricle outflow tract (RVOT). The study to the MPA and to an orientation along the RVOT inspired a methodical analysis of flow patterns in the whole PA structure in healthy volunteers (Bächler *et al* 2013). The main finding is that the flow into the MPA is not a simple pipe flow with parallel streamlines. Instead the flow appears to be helical in the MPA and right pulmonary artery (RPA), in the form of counter-rotating helices in the MPA that contributed mainly to the right-handed helical flow observed in the RPA. The phenomenon of helical flow in the MPA and the RPA of healthy volunteers is debated. The incidental finding of Kilner *et al* (1993) affirmed the existence of right-handed helical flow in the RPA. However, Francois *et al* (2012) assessed differences in haemodynamics in the right heart and PA between 10 healthy volunteers and 11 patients with repaired tetralogy of Fallot, and reported conclusively laminar flow in the MPA and the left pulmonary artery (LPA) of all volunteers and in the RPA of 6 volunteers. Moreover, increased helical and vortical flow patterns appeared to be associated with the PA of repaired tetralogy of Fallot patients, in agreement with the findings of Geiger *et al* (2011).

Schäfer *et al* (2017) suggested that helicity and vorticity can be used as indicative indices conveying RV function. Decreased helicity and vorticity in the PA is correlated with the increased pulmonary stiffness and compromised RV ventricular/vascular coupling ratio. It suggests that a relationship exists between the RV and quantitative haemodynamic flow indices in the PA. Additionally, helicity is quoted as having the best diagnostic potential, due to its diagnostic accuracy exceeding that of other standard MRI measures. Even so, the study was restricted to the examination of only the MPA and the RPA due to the limited 4D flow MRI acquisition window, imaging incomplete portions of the LPA. This is similar to Reiter *et al* (2008), in failing to produce a complete analysis of the PA vasculature.

Helicity and vorticity in the PA bifurcation of healthy paediatric subjects has also been explored. Using computational fluid dynamics, Capuano *et al* (2019) showed that the bifurcation anatomy was haemodynamically efficient when the boundary layer separation and turbulent flow (hence reduces energy loss) is minimised during flow acceleration phases when curvature of the geometry is sufficiently small, whilst separation does occur in the same anatomy during flow deceleration phases. Helical flow was also reported in the RPA, similar to Bächler *et al* (2013) and Schäfer *et al* (2017), and its formation mechanism was likely to be triggered by the MPA curvature. It is known that pipe with sufficient curvature induces helicity spontaneously from a initially parallel flow, similar to the Dean vortex observed in aortic flow in the descending aortic arch (Timité *et al* 2010) albeit the curvature in the MPA is milder. However, we will show that significant helicity develops early (upstream) in the MPA, originated from the RVOT and influenced by the pulmonary valve.

Despite separate studies into the flow patterns in the PA and quantitative haemodynamic indices, the link between the RV and the PA quantitative measures provides the basis for further investigation. The cause of the two counter-rotating helices observed by Bächler *et al* (2013) in the MPA remains unclear. There has not been, as far as the authors are aware, an investigation into the relationship among haemodynamic quantities, viz. helicity,

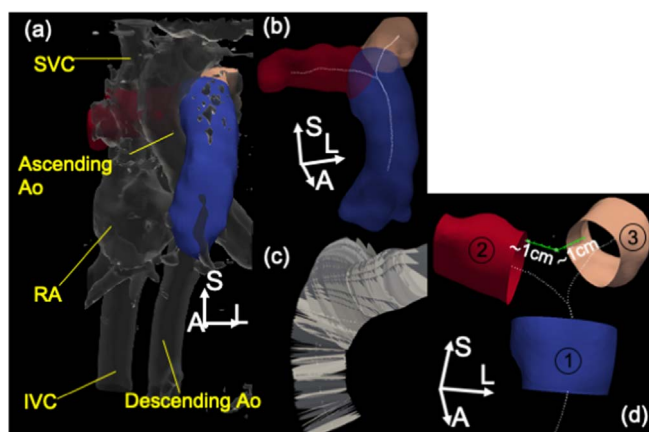


Figure 1. (a) Illustration of the segmented PA structure. SVC; superior vena cava, RA; the right atrium, IVC; inferior vena cava, Ao; aorta. (b) The separated PA with the traced centreline points. (c) The cross-sectional plane perpendicular to the local centreline trajectory shown in (b). (d) Illustration of the branch sections starting approximately at 1 cm downstream of the bifurcation point; MPA ⊙, RPA ⊙ and LPA ⊙. Coordinate system: left (L), anterior (A), superior (S), so for all the other relevant figures.

entropy (a measure of the vorticity strength), KE and energy dissipation rate, in the PA and the RV and their association with the origin of the previously observed helices in the PA vasculature.

The purpose of this study is to assess the relationships between the aforementioned quantitative measures, in company with the visualisation analysis of blood flow patterns within the PA and between the RV and the PA, to elucidate normal ventricular-vascular behaviour and deduce blood flow pattern-related measures in a structurally normal heart. The relevance of this study is the advancement in the understanding of the normal flow in the PA, which offers a reference to the community to develop the next generation more reliable diagnostic tools and treatment plans for dysfunction of the right heart.

2. Methods

2.1. Study population and magnetic resonance imaging

The study population and the 4D flow MRI technique adopted by the current study were detailed in Parikh *et al* (2017) and Dewhurst *et al* (2020). In total 18 healthy participants (seven male, age range 21–50) with structurally normal hearts were recruited through advertisement within Newcastle Hospitals NHS Foundation Trust and all participants provided informed written consent.

The MRI was conducted at 3.0 Tesla (Achieva, Philips Best, The Netherlands) with a 6-channel cardiac array. Short axis, horizontal and vertical long axis and 4-chamber views retrospectively-gated steady-state free precession sequences were obtained during breath holding (Hollingsworth *et al* 2012). 4D flow MRI was carried out implementing a retrospectively ECG-gated and respiratory gated turbo field echo sequence. Field of view: 240 mm (antero-posterior) \times 240 mm (caudad-cranial) \times 142 mm (left-right), spatial resolution: $3 \times 3 \times 3$ mm³, temporal resolution: 50–55 ms, 20 cardiac phases. A respiratory navigator was used to minimise motion artefact. Phase errors introduced by eddy currents and Maxwell terms were corrected during the reconstruction process (Carlsson *et al* 2011).

2.2. Data analysis

The segmentation of the PA and the RV (including the RVOT) was conducted semi-automatically following an in-house developed procedure considering both the velocity and MR magnitude data. The software utilised were ParaView, ITK-Snap and Matlab. For each subject, the RV segmentation was performed on all the 20 cardiac phases. The PA segmentation was performed at the peak systolic phase, which was then used as a mask for each phase of the cardiac cycle. In this way, the PA was treated as a rigid body whose shape deformation through the cardiac cycle is neglected. Schäfer *et al* (2017) reported the relative change of the cross-sectional area in the PA can be as high as 29% between peak diastole and peak systole, the assumption of stiff PA acting is however in line with Capuano *et al* (2019), who applied the result of minimal differences to the aorta flow field when considering compliant and rigid wall models to the PA (Jin *et al* 2003). Figure 1(a) illustrates the segmented PA in relation to the selected anatomic structures nearby. The centreline was then computed and traced along the PA structure shown in figure 1(b), from which cross-sections perpendicular to the the local centreline orientation was

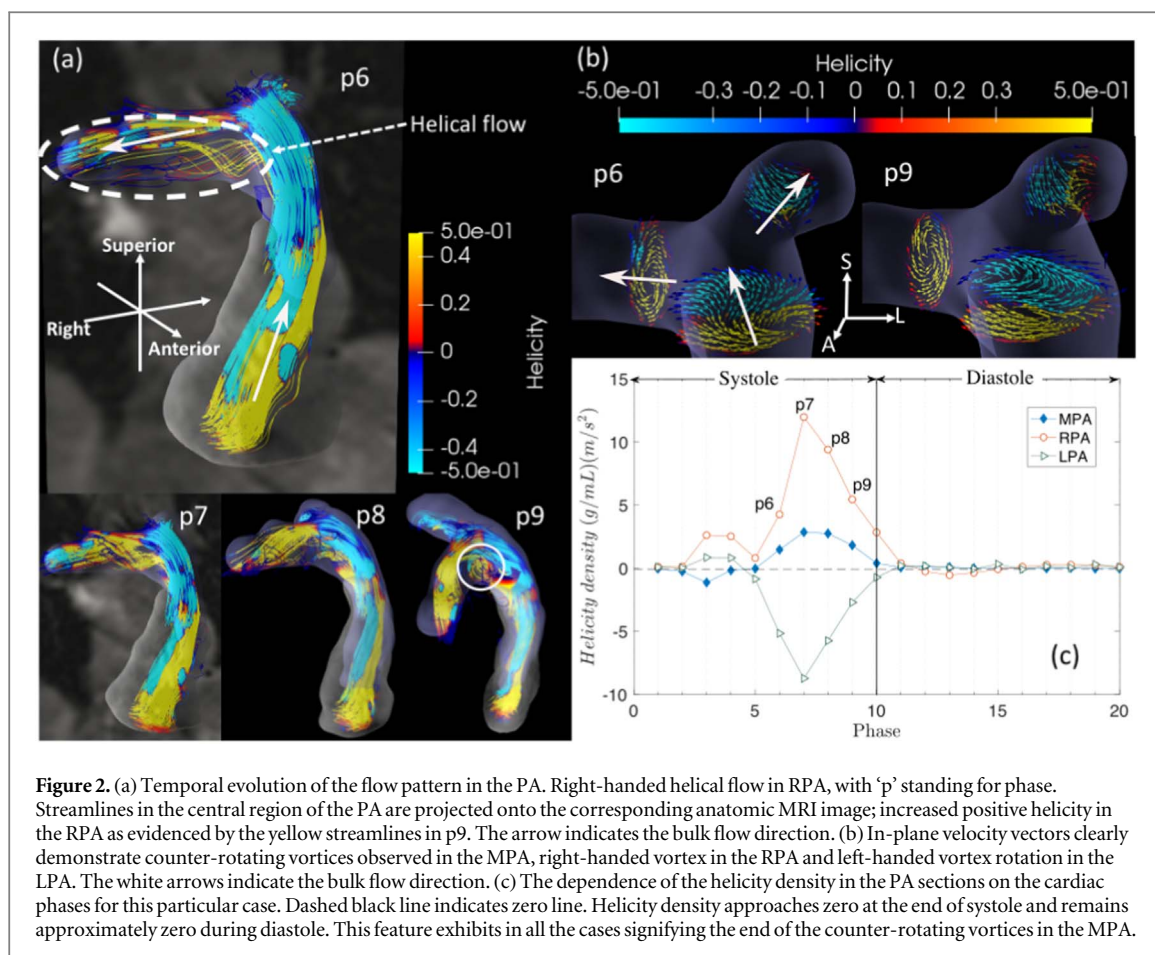


Figure 2. (a) Temporal evolution of the flow pattern in the PA. Right-handed helical flow in RPA, with ‘p’ standing for phase. Streamlines in the central region of the PA are projected onto the corresponding anatomic MRI image; increased positive helicity in the RPA as evidenced by the yellow streamlines in p9. The arrow indicates the bulk flow direction. (b) In-plane velocity vectors clearly demonstrate counter-rotating vortices observed in the MPA, right-handed vortex in the RPA and left-handed vortex rotation in the LPA. The white arrows indicate the bulk flow direction. (c) The dependence of the helicity density in the PA sections on the cardiac phases for this particular case. Dashed black line indicates zero line. Helicity density approaches zero at the end of systole and remains approximately zero during diastole. This feature exhibits in all the cases signifying the end of the counter-rotating vortices in the MPA.

constructed as shown in figure 1(c), enabling the calculation of flow rate, similar to Sullivan and Trainor-Guitton (2019).

Flow patterns were investigated in the PA and the RV using streamlines coloured by helicity to visually depict the flow motion, along with the direction of the flow rotation. The calculation of the haemodynamic quantities followed Dewhurst *et al* (2020). The relevant equations involved are summarised in the appendix, where the volumetric integrals of KE, enstrophy, helicity and dissipation rate are denoted by E_k , E_r , H and E_e , respectively. Due to the relatively low spatial resolution with respect to the PA size, in order to improve the flow visualisation quality and the accuracy of volumetric integration, the raw data was spline interpolated using Matlab to a refined resolution of 1 mm^3 voxel. We were interested in the volumetric density of these quantities instead of the absolute magnitude. In this way, we removed the structural size dependency. It was done by normalising the quantities calculated in equations (1), (2), (3) and (6) by the volume of the segmented region of interest. Length of approximately 2 cm were taken from the MPA and the proximal LPA and RPA, as seen in figure 1(d), as the segmented regions. The LPA and the RPA sections initiated approximately 1 cm from the bifurcation point to minimise the cross interference, as the distance from the bifurcation acted as a reliable marker and assured measurements from the same location across subjects (Wehrum *et al* 2016). The MPA section started approximately 1 cm downstream of the pulmonary valve. Pearson correlation analysis was then performed in the PA vasculature to investigate the interrelationships of KE, helicity, enstrophy and dissipation rate etc.

3. Results

3.1. Flow patterns

A right-handed helical pattern is observed in all the cases studied (having different intensities in different cases), with a clear example shown in figure 2(a), where the growth of the helical flow in the RPA is tracked from phase 6 to 9. The RPA contains both positive and negative sensed helicity (clockwise and anti-clockwise rotation at a given bulk flow direction) at phase 6 and as the helix develops to phase 8, the helicity intensity of the streamlines becomes stronger, indicating increased cohesiveness and linkage within the flow. At phase 9, additional recirculating flow emerges at the top of the MPA (as highlighted) and the right-handed helix descends further into the MPA without protruding into the RPA. From the RV to the MPA, two strips of opposing helix are

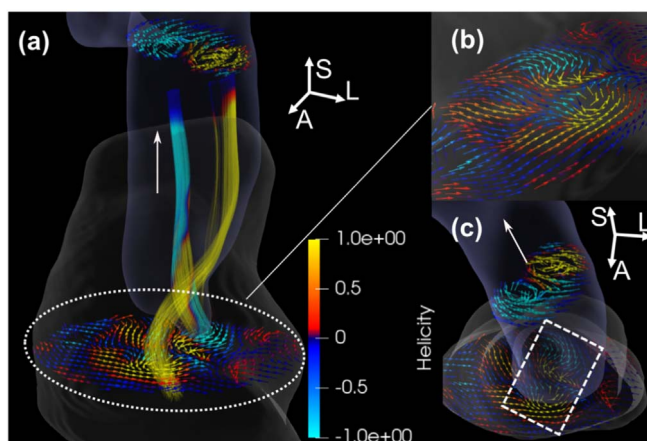


Figure 3. Streamline pattern and sectional velocity vectors coloured by helicity intensity in the RV and the MPA near peak systole (phase 7 for this particular case). (a) Coherent helical streamlines of opposite helicity are likely emanating from the RV but affected by the pulmonary valve where the stream passes the valve annulus. (b) Close-up view of cross-sectional slice highlights vortical patterns of negative (cyan) and positive (yellow) helicity by in-plane velocity vectors, in the RV under the RVOT. (c) View into the RV through the RVOT capturing the locations of the vortices in the MPA relative to the RV. The dashed box encloses the two counter-rotating vortices in the RV. The white arrows indicate the bulk flow directions.

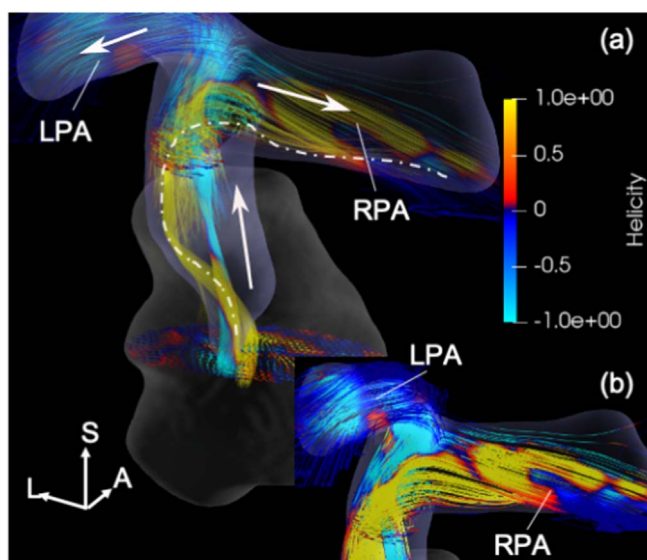


Figure 4. Helical streamlines in the PA bifurcation region; the same case and phase number as figure 3. (a) The white dotted line indicates the emergence of the flow from the posterior-left of the MPA curls to the RPA. (b) Streamlines into the LPA and the RPA. The white arrows indicate the bulk flow directions.

maintained. However, beyond the bifurcation, helical flow with positive helicity organises in the RPA and that with negative helicity in the LPA. These findings are qualitatively in agreement with Capuano *et al* (2019). Figure 2(b) illustrates more clearly the composition of opposing helix in the MPA flow, with counter-rotating vortices winding in the MPA. Right-handed rotation of flow in the RPA and left-handed rotation in the LPA are also depicted by the vectors, particularly clearly in the case. The latter can be observed more clearly in figure 2(a) phase 9. The sectional flow rotation centre in the RPA shifts closer to the central region of the RPA branch from phase 6 to phase 9 in figure 2(b) and forms a tighter spiral in keeping with the increased cohesiveness of the streamlines recorded in figure 2(a). More enclosed vortical patterns are established in the MPA by phase 9. It must be clarified that the flow streamlines in figure 2(a) appear largely parallel at phase 9. This is because of the stronger streamwise velocity component than the in-plane component. Nevertheless, the RPA was not always confined to right-handed helical flow. It is noted that four cases having strong negative helicity density in the RPA at peak systolic phases; see the supplementary materials (available online at stacks.iop.org/PMEA/42/025005/mmedia).

Table 1. Cross-sectional averaged flow quantities. All entries are in the format of average \pm standard deviation.

Branch	Stroke volume (ml)	Equivalent diameter ^a (cm)	Peak stroke velocity (cm s ⁻¹)
MPA	72.72 \pm 30.50	2.80 \pm 1.29	50.91 \pm 22.68
LPA	29.02 \pm 17.14	2.00 \pm 0.95	40.43 \pm 18.40
RPA	42.14 \pm 17.46	2.17 \pm 1.00	44.67 \pm 21.62

^a Measured at the peak systolic phase.

The helicity density calculated in the PA vascular domain (MPA, RPA and LPA), by equation (3) and normalised by the domain volume, over the cardiac cycle in figure 2(c) echos the helical structure observed in (a) and (b). The onset of helical flow and counter-rotating vortices in the MPA occurs at a phase prior to the peak helicity density and remain visible until phase 10, which marks the end of the ventricular systole. A similar flow pattern is observed in all the cases studied, with the emergence of the counter-rotating vortices at or near the peak helicity density and their strength maintained until the end of systole when the blood stream ejection fades. There is also an appreciable change of helicity polarity in the MPA during systole (see phase 3 in this case). Similar observations are made in 12 (out of 18) cases, although most cases show weak negative overall helicity at peak systole; see supplementary materials. This particular case also shows clear positive overall helicity density in the RPA and negative helicity in the LPA in figure 2(c). Figure 3(a) depicts regional velocity vectors on a sectional plane in the RV below the RVOT and two bundles of streamlines highlighting the flow pattern in the central MPA. For this particular case, the appearance of the counter-rotating vortices in the MPA and vortical patterns of strong helicity in the RV starts to emerge at phase 5 (figure not shown) and by phase 7 (as shown), the development of helical flow in both the MPA and the RV is clearly reflected by the formation of in-plane vortices, with that in the RV magnified in (b). From phase 8 the counter-rotating structure in the MPA diminishes and vanishes in phase 9 (the end of the systolic phase), paired with a collapse of the rotating flow in the RV. Figure 3(c) highlights the two in-plane counter-rotating vortex pattern in the RV (in the dashed box) and the shift in position of the corresponding vortex centres in the MPA.

Flow helicity emanating from the left posterior side of the MPA is found to contribute to the helical flow in the RPA spanning the same duration as first reported by Bächler *et al* (2013). Figure 4 is included to emphasise the streamline pattern in the area. The portion of the flow in the RPA that appears to have the highest positive helicity intensity (figure 4(b)) comes from the strong helical flow in the left posterior side of the MPA, which further stems from the upstream of the MPA and the RV (figure 2(a)). Qualitatively visible in figure 4, the flow in the PA vasculature exhibits asymmetry of flow distribution at bifurcation. That is, flow on the very left side of the MPA could enter the RPA (in a helical manner), as indicated by the white dashed line. In total 14 (78%) of the studied population exhibit similar flow pattern. The four exceptional cases are also the cases having clear negative helicity in the RPA at peak systole and they are displayed in the supplementary materials.

3.2. Mean flow quantities

Some of the flow statistics in the MPA, the LPA and the RPA are given in table 1. The net forward volumetric flow rate were calculated through a perpendicular plane located in the mid-plane of the MPA and in the proximal LPA and RPA branches. The flow rate in the MPA, when compared with the sum of the net forward flow in the LPA and RPA, shows a good agreement, with a minor mean difference of 1.6 ml per stroke. On the other hand, the blood flow distribution ratio to the RPA and the LPA is about 1.4, in consistent with Cheng *et al* (2005).

The ratio of the equivalent diameter of the MPA and the LPA, $\psi(M|L) = 1.41 \pm 0.14$. The size of the RPA is consistently about 10% larger than the LPA for all the cases, with their equivalent diameter ratio $\psi(R|L) = 1.09 \pm 0.11$. Four cases have their RPA slightly smaller, with the lowest $\psi(R|L) = 0.93$ and the other three $\psi(R|L) \gtrsim 0.97$. Combining the flow rate results, it can be deduced that the cycle averaged bulk flow velocity ratio in the RPA to the LPA is $U(R|L) = 1.39 \pm 0.46$. Four cases have their ratio slightly less than unity, but all with $U(R|L) \gtrsim 0.9$. The maximum and minimum values of $U(R|L)$ are 2.4 and 0.51 respectively.

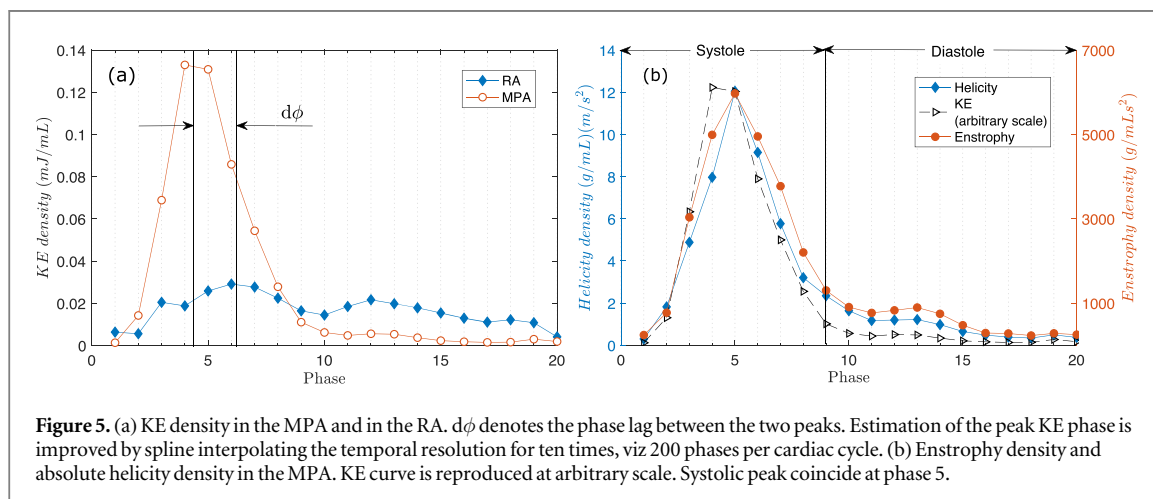
From the KE density and the segmented PA cross-sectional areas, it is possible to calculate the KE flux (KE_f) through the three PA sections, from which the cycle averaged KE loss, ΔKE , can be quantified, where $\Delta KE = KE_f(MPA) - KE_f(RPA) - KE_f(LPA)$. It is found that the ratio $\Delta KE/KE_f(MPA) = 0.18 \pm 0.15$. There are three cases having small negative ΔKE values, which are unphysical. This is likely due to the measurement noise or segmentation uncertainty. These negative values are removed when calculating ΔKE .

Table 2. Correlation of the same flow quantity between different PA sections.

Meas. 1	Meas. 2	$R(P)$ value	Meas. 1	Meas. 2	$R(P)$ value
E_{kMPA}	E_{kLPA}	0.55(0.02)	H_{MPA}	H_{LPA}	0.15(0.56)
E_{kMPA}	E_{kRPA}	0.43(0.07)	H_{MPA}	H_{RPA}	0.58(0.01)
			H_{MPA}	$H_{LPA} + H_{RPA}$	0.44(0.07)

Table 3. Association between different quantitative flow measures in the same PA section. All quantities listed under Measure 1 and Measure 2 are calculated from densities at the peak systolic phase. H denotes helicity, E_r enstrophy, E_k kinetic energy, E_c dissipation rate. Correlations with P value larger than 0.05 is denoted as ns (insignificant). The exact P value is not quoted for $P < 0.001$.

Meas. 1	Meas. 2	$R(P)$ value	Meas. 1	Meas. 2	$R(P)$ value
H_{MPA}	E_{rMPA}	0.85 (<0.001)	E_{cMPA}	E_{kMPA}	0.53 (<0.001)
H_{LPA}	E_{rLPA}	0.83 (<0.001)	E_{cMPA}	H_{MPA}	0.72 (<0.001)
H_{RPA}	E_{rRPA}	0.60 (0.009)	E_{cMPA}	E_{rMPA}	0.69 (0.0016)
E_{kMPA}	E_{rMPA}	0.75 (<0.001)	E_{cLPA}	E_{kLPA}	ns
E_{kLPA}	E_{rLPA}	0.69 (0.0014)	E_{cLPA}	H_{LPA}	0.61 (0.007)
E_{kRPA}	E_{rRPA}	0.60 (0.0083)	E_{cLPA}	E_{rLPA}	0.60 (0.009)
H_{MPA}	E_{kMPA}	0.88 (<0.001)	E_{cRPA}	E_{kRPA}	ns
H_{LPA}	E_{kLPA}	0.71 (<0.001)	E_{cRPA}	H_{RPA}	ns
H_{RPA}	E_{kRPA}	ns	E_{cRPA}	E_{rRPA}	0.84 (<0.001)

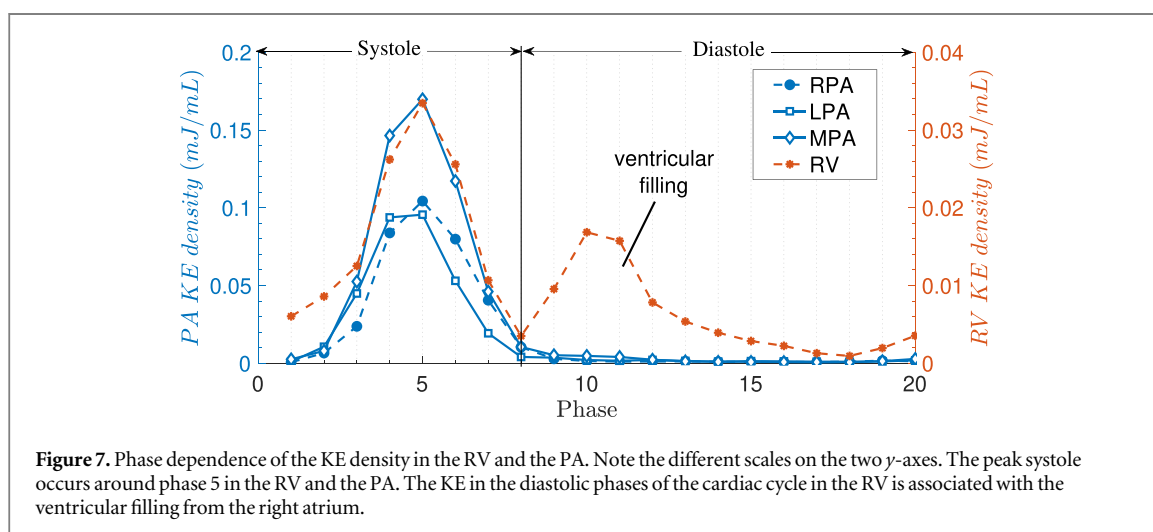
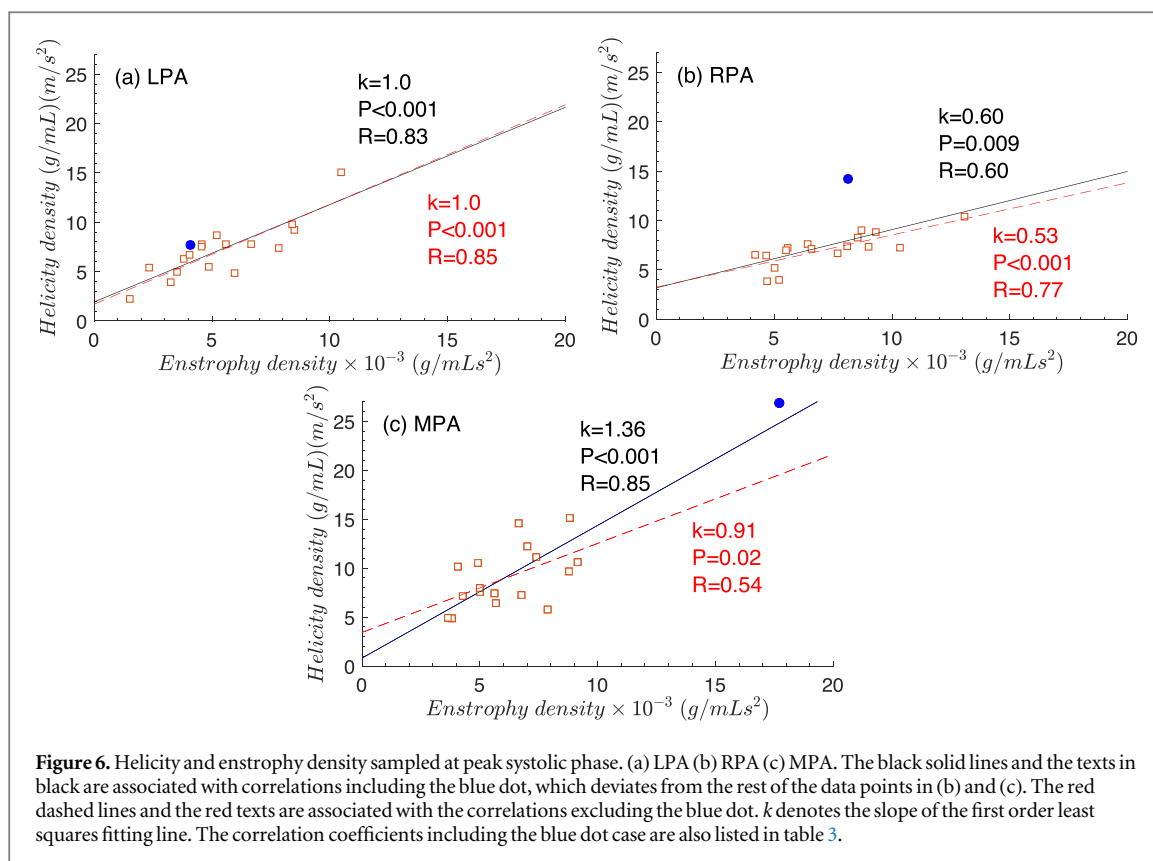
**Figure 5.** (a) KE density in the MPA and in the RA. $d\phi$ denotes the phase lag between the two peaks. Estimation of the peak KE phase is improved by spline interpolating the temporal resolution for ten times, viz 200 phases per cardiac cycle. (b) Enstrophy density and absolute helicity density in the MPA. KE curve is reproduced at arbitrary scale. Systolic peak coincide at phase 5.

3.3. Correlations of flow quantities in the PA vasculature

We focus on the correlation of flow quantities at peak systolic phase. We also assume that the flow evolves rather smoothly through the nearby phases. Additionally, the magnitude of helicity density is used to remove the polarity-dependency. The effect of helicity polarity has been shown in the previous section. Correlations between the quantities presented below are not always expected to be significant for an arbitrary flow in a PA alike anatomy.

In terms of the correlation of the same flow quantity between different PA sections, weak or moderate correlations are obtained and they are tabulated in table 2. Since the correlations are mostly insignificant, the exact values of coefficients are listed. The correlation of the MPA with the LPA and the RPA are both insignificant. The maximum KE density occurs in the MPA for 13 out of the 18 cases. Of the remaining five cases, the maximum KE density is attributed to the LPA in two cases and the RPA in the rest. Note that these are density, where the size difference is eliminated. Enstrophy density reflects no clear correlation between the PA sections with ($-0.01 < R < 0.2$; $P > 0.47$), suggesting that rotational energy is not well convected from the MPA to the L/RPA, plausibly because of the bifurcation affects the rotational energy. Also no significant correlation can be found between the helicity density in the MPA and the LPA or the MPA and the sum of the LPA and the RPA. Better helicity correlation is found in the MPA and the RPA, which implies that helical flow is convected favourably from MPA to the RPA compared to the LPA. This is qualitatively supported by the flow visualisation in figures 2(a) and 4.

Correlations between different haemodynamic quantities in the same PA section are listed in table 3. Figure 5(a) shows the KE density in the MPA and the right atrium (RA) of a typical case. RA data is taken from Dewhurst et al (2020). Not surprisingly the peak KE in the MPA is much higher (nearly five times) than that in



the RA. However, because of the residual KE in the RA over the diastolic phases, the cycle averaged KE densities is less different, with the RA on average having about 20% less than that in the MPA. Moreover, the peak atrium diastole (the peak of the RA KE density) consistently lags the peak systolic phase of the MPA, which in this case is phase 5, commencing at the same time as the formation of the counter-rotating vortices in the MPA, as demonstrated in section 3.1. This phase lag, as demonstrated by $d\phi$ is consistent in all the study cases to be 0.86 ± 0.29 cardiac phase. Figure 5(b) highlights a similar pattern between helicity and enstrophy as well as KE in the MPA. The strong positive correlation among the three quantities is also shown in table 3. The helicity and enstrophy are approximately synchronised, which is a reflection of organised unidirectionally rotational flow, according to their mathematical definitions. The KE and the enstrophy are aligned better over the accelerating phases, but the latter lags the KE curve after the peak KE density (around phase 5), i.e. KE diminishes more quickly than the rotational energy. There is also non-negligible rotational energy remaining in the diastolic phases. This is a common finding in 14 cases studied. For this particular case, the lag is about 0.05 cardiac phase (50–55 ms) at the end of systole.

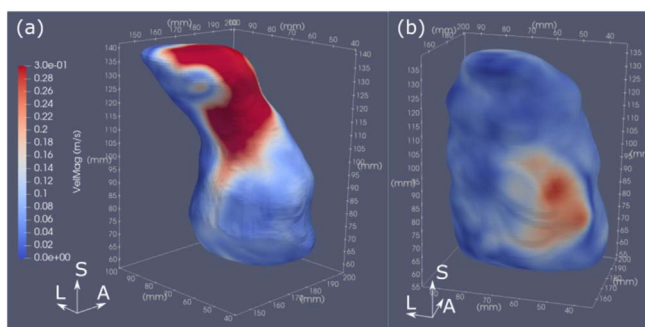


Figure 8. Velocity magnitude contour plot on the RV surface for a typical case. (a) Peak systole with the concentration of high KE around the RVOT. (b) Peak diastole with a lower KE magnitude in region adjacent to the ventricle inlet/tricuspid valve and below RVOT. Coordinate axis L: left, A: anterior, S: superior.

Table 4. Association between quantitative measures in the RV and the PA. All quantities listed under Measure 1 and Measure 2 are densities. The RV and the MPA quantities are both taken at their peak systole phases, which can be slightly different in some cases. Correlations with P value larger than 0.05 is denoted as *ns* (insignificant). The exact P value is not quoted for $P < 0.001$.

Meas. 1	Meas. 2	$R(P)$ value	Meas. 1	Meas. 2	$R(P)$ value
H_{MPA}	H_{RV}	0.78 (<0.001)	E_{eRV}	E_{tRV}	0.98 (<0.001)
E_{tMPA}	E_{tRV}	ns	E_{eRV}	E_{kRV}	0.85 (<0.001)
E_{kMPA}	E_{kRV}	0.74 (<0.001)	E_{eRV}	H_{RV}	0.86 (<0.001)

The relationship between helicity and enstrophy within the PA is displayed in figure 6. The reasonable correlation indicates that the helical flow structure increases the turning of the flow, causing vorticity and therefore enstrophy to grow due to the increased rotation of the flow. It should be noted that one off-trend case denoted by the blue point causes the correlation to be weaker in the RPA as shown in table 3 (comparing the first three entries). Correlations without this off-trend case are also presented in figure 6, which is strengthened slightly for the RPA and weakened for the MPA. The raw data are provided in the supplementary materials.

3.4. Correlations between the PA and the RV

The relationships between quantitative flow haemodynamic metrics between the RV and the PA are given in table 4. Conservation of both helicity and KE densities between the RV and the MPA is supported by their reasonable linear correlations. This is also noteworthy, in light of the weaker correlations of helicity and KE densities between the MPA and the PA branches shown in section 3.3. The rotational energy (enstrophy) does not appear to be correlated, similar to the PA vasculature.

The behaviour of KE observed in the PA and the RV is compared in figure 7 for a typical case. The contraction of the RV myocardium inputs greater magnitude of KE to the confined MPA causing the flow passing from a larger area into a smaller area abruptly inducing a great increment in velocity magnitude. The PA peak systolic phase coincides with that of the RV and the trend of KE in the RV is mirrored by the MPA during systole. This confirms that KE in the RV is directly transferred to the MPA. KE is negligible during diastole in the MPA but displays a clear secondary peak in the RV. This is because of the closure of the pulmonary valve during diastole to prevent backflow, and therefore the flow energy in the RV is isolated and arises from ventricular filling, as blood flows from the RA to the RV. The RV KE systolic peak is higher than the diastolic peak for 11 out of 18 cases, in agreement with van der Geest and Garg (2016), who reported a higher KE systolic peak in the RV over the cardiac cycle for healthy volunteers.

In order to better understand the high degree of correlation of KE density between the RV and the MPA, figure 8(a) is presented to show the RVOT region during the peak systole, where the highest KE intensity is found to occur. Since the RVOT, which is included in the RV segmentation, is the inlet of the MPA, the flow here is the main reason for the good correlation result. In comparison, the KE peak during diastole, which has a lower intensity, occurs in the region adjacent to the ventricle inlet/tricuspid valve and below RVOT; see (b).

Dissipation rate exhibits stronger correlation with the other flow quantities in the RV as shown in table 4, especially for the enstrophy, similar to the RA (Dewhurst et al 2020), where the flow are more three-dimensional. In contrast, in the PA vascular domain, under the influence of the bulk unidirectional flow, the correlation between the dissipation rate and other quantities, e.g. enstrophy density, is much weaker as shown in table 3.

4. Discussion

This study presents non-invasive assessment of flow patterns in the PA vasculature using 4D flow MRI. Both qualitative flow visualisation and quantitative correlation analyses of flow dynamic quantities were carried out. As far as the authors are aware, the correlation between the quantitative metrics, e.g. enstrophy, helicity and dissipation, in the PA in relation to the helical flow patterns observed are established for the first time. Special focus is on the peak systolic phase where the peak ejection occurs in the PA vasculature. In order to remove the PA size difference among the study cases, the flow quantities are all volumetrically normalised to represent densities or local intensity. We observed and quantified the significant flow asymmetry in the PA flow, in terms of asymmetric flow rate and various haemodynamic intensities in the LPA and the RPA, as well as the weak overall helicity bias in the MPA, which reflects the weak asymmetric flow rotation.

Comparing to the MPA stroke volume reported in Ugander *et al* (2009), our data presented in table 1 has appreciably lower mean values and larger standard deviations. This is mainly because of the larger age range of the studied cohort. No clear correlation with gender is noticed. The different temporal and in-plane spatial resolution used in Ugander *et al* (2009) may also contribute to the difference. The MPA mean stroke volume of the present study is more similar to an earlier data set (Cheng *et al* 2005). The flow split (ratio) between the LPA and the RPA is also consistency with, but deviates slightly from that reported in Bächler *et al* (2013), which is about 1.2. This could also be the result of the different resolution at which measurements are acquired. The assumption of non-compliant PA could also contribute but is believed to be a minor factor as discussed above.

It is worth mentioning that the spatial resolution of the present study is isotropically 3 mm, similar to Schäfer *et al* (2017). Many studies adopted higher in-plane resolution but lower resolution in the direction normal to the main stream, to compensate for the total MR scan time. This might be advantageous in measuring flow rates in arteries and/or veins, but it causes problem in calculating higher order quantities like vorticity, unless special treatment to the resolution anisotropy is applied.

The cycle mean KE loss (ΔKE) in the studied population is found to be about 18% of the KE in the MPA, up to about 30%. The main contributor of this loss is believed to be the bifurcation anatomy of the PA where the flow stream in the MPA experiences strong adverse pressure gradient at the bifurcation junction during flow acceleration and flow separation (and therefore turbulence to dissipate KE) originates from the inferior corner of the L/RPA—MPA junction during flow deceleration (Schäfer *et al* 2017, Capuano *et al* 2019). Although the frictional loss on the artery wall may also contribute, it is believed to be insignificant compared to the former effect. The amount of KE loss mainly depends on the local PA bifurcation geometry. To quantify this dependency is left to a future study. On the other hand, abnormally high KE flow in the PA can damage the blood vessels in the lungs and be more susceptible to developing acquired PH. Pulmonary flow restriction sometimes needs to be applied, e.g. to very young infants having congenital heart disease by PA banding (Sharma 2012).

Given an instantaneous contraction pressure applied by the RV, the volumetric KE density, hence the bulk velocity in the PA is mainly determined by the afterload, i.e. the resistance or the pressure in the lung circulation. Since the loss coefficient for the splitting flow at a T junction is typically larger than unity for common pulmonary bifurcation angles (Benedict 1980), the steady Bernoulli relation (Batchelor 2000)⁵ indicates that at peak systole the pressure at the MPA is always higher than that in the lung, which makes physical sense. We cannot conclude whether the five cases having higher KE in the LPA or the RPA means lower pressure in the left or the right lung respectively, i.e. asymmetric lung pressure, because the exact loss coefficient is highly anatomically dependent and is hard to quantify. To derive the pressure gradient field from the available velocity field (Gan *et al* 2012), although possible, is also beyond the scope of the present study.

The well correlated haemodynamic quantities evidenced in table 3 support the flow visualisation in section 3.1. That is, around the peak systole, the flow in the three PA sections is not of a simple parallel type. The flow is highly organised in a helical manner, similar to the superior and inferior vena cava flow (Dewhurst *et al* 2020). The quicker rising and slower diminishing of enstrophy than KE as shown in figure 5 seems to imply that the rotational flow is well convected by the main stroke stream to the MPA and dissipated more slowly than the pulsatile peak. The interaction of the main stream and the pulmonary valve also contributes as an extra source of rotational energy input as vortices shed from the leaflets (Kheradvar and Pedrizzetti 2012). Its contribution however is hard to quantify given the measurement resolution. The residual rotational energy in diastole phases shown in figure 5 suggests that small scale rotational flow remains locally without being advected downstream in the MPA, i.e. the flow is not entirely stationary when pulsatile peak passed. However, it must be acknowledged

⁵ At peak systole, the local maxima of KE density implies that the velocity gradient with respect to time or phase is near zero (although the limited temporal resolution is less likely to capture the true maximum phase). The same argument also supports temporarily rigid pipe assumption for the PAs. Also since the flow rotation is weak compared to the bulk flow velocity, the relation between the pressure gradient and the velocity along streamlines in the central part of the arteries can approximately be described by the steady Bernoulli equation.

that this could be contaminated by the ‘phase-averaged’ nature of the 4D flow MR technique in calculating vorticity, which overestimates the very small velocity gradients.

Classical turbulence theory states that dissipation is associated with rotating eddies at small scales and hence the dissipation estimation in equation (4). Table 3 shows that KE density consistently has the weakest correlation with dissipation in the PA branches, comparing to enstrophy and helicity. This means that enstrophy is the primary means of energy dissipation throughout the PA, inline with this theory. The linear correlation between the absolute helicity density and energy dissipation rate density in the LPA and the MPA as shown in table 3 is, on the other hand, expected, as firstly explained by the theory, and secondly it was supported by Schäfer *et al* (2017) that helicity is indicative of energy dissipation. It is also in line with the way dissipation is estimated; see the appendix. Theoretically, dissipation is more accurately calculated by resolving to the dissipative length scales, which in the case of PA channel flow, would be in the order of 10^{-2} mm (Davidson 2015). It is a formidable target to achieve for any non-invasive measurement technique.

The slope of the first order least squared fitting line (k) of helicity and enstrophy, which is appreciably different in the three PA branches as shown in figure 6, could provide more information for the general PA flow type in a structurally normal heart. For the same enstrophy, hence vorticity (ω) magnitude, the bulk streamwise flow is stronger in the LPA than in the RPA. On the other hand, considering the peak flow velocities in the three branches listed in table 1 or the values of the data points, it may be concluded that the vorticity intensity in the RPA is about 20% higher than that in the LPA, and 8% higher than in the MPA. For pipe-like PA flows, enstrophy can be understood as velocity normalised manifestation of flow helicity, as it eliminates the bulk flow velocity effect, which is approximately unidirectional. In terms of helicity itself, it is about 5% higher in the RPA than the LPA. Comparing with figure 2(c), which takes into account the helicity polarity, it can be inferred that in the MPA the two counter-rotating helical flow streams may wind together without clear bias. In agreement with Bächler *et al* (2013), the duration of their existence spans from near or at the peak systole to the late systole. If the counter-rotating streams are of similar intensity, their effect may cancel each other and results in an overall helicity of low magnitude. This is also supported by the weaker correlation in the MPA shown in figure 6(c) (if the off-trend case is excluded) and suggests that the flows in the LPA and the RPA exhibit a feature of more unidirectional rotation.

Indeed, in the LPA and the RPA, 14 cases show that the flow helix is unidirectional at peak systole, viz. positive helicity in the RPA and negative helicity in the LPA as shown in figures 2(b) and (c), five of them being weak. This indicates an symmetric sense of rotation. That is, since the bulk velocity directions are opposite, positive and negative values of helicity density express opposite directions of flow swirl viewing from the bifurcation but the same vorticity direction (by the right-hand rule) viewing along the left-right axis; see equation (3). In this sense, the rest cases shows asymmetric rotation in the LPA and the RPA, with two cases being clear; see the supplementary materials.

These features seem to be linked to the positive and negative helical streams from the MPA, respectively, a distance upstream of the bifurcation (figure 4). The 3 (of the 4) cases displaying negative helicity in the RPA near the peak systole mentioned in section 3.1 happen to be associated with *strong* negative overall helicity in the MPA. This seems to be supported by the hypothesis in Bächler *et al* (2013) that part of the helical flow in the RPA originates from the left posterior MPA. Indeed, figures 4(a) and 2(a) highlight the helical pattern formed in the RPA emerging from the left-hand side of the MPA and exhibiting a stronger helical pattern than the remaining flow directed into the RPA. This parallels with the helical structure at the right inner wall of the MPA and into the RPA reported by the *in silico* study of Capuano *et al* (2019). However, that study was limited to the PA bifurcation, which accounts for the right inner wall of the MPA only and not the earlier propagation of the flow from the left side of the MPA. Support is also provided by the better correlation of the helicity density between the RPA and the MPA as given in section 3.3, as well as the higher flow rate (table 1) and higher enstrophy density (figure 6) in the RPA, compared to the LPA.

Two in-plane vortices of opposite sense of rotation are also noticed in the RV, coupled to those in the MPA of matching rotation via streamlines (figure 3). This indicates the rotation of the flow along the RVOT. The focus on the two flow streams arising from the vortices in the RV in figure 3(a) indicates that the helical nature of the flow is difficult to visualise with streamlines alone because of the large bulk flow velocity flux in the MPA during peak systole. Although Capuano *et al* (2019) suggested that the RPA helical pattern originates from the MPA curvature, figure 3 implies that the helicity in the MPA is probably due to the torsional motion and recoiling of the anisotropic shaped RV during contraction at the peak systolic phase (Bächler *et al* 2013) and is also influenced by the boundary layer shed to the MPA stream as the flow goes through the pulmonary valve annulus. Near the peak systolic phase, when the pulmonary valve opens at its maximum extent (so for the annulus opening), the instantaneous flow flux is high. The helical nature of the flow in the RV is delivered to the MPA through the annulus. This is also confirmed quantitatively, by a strong positive linear correlation connecting the absolute helicity density in the RV to the MPA; see table 4.

Of note is the stronger KE density correlation between the RV and the MPA, compared to those between the PA branches given in section 3.3. Regions of high KE are located along the RVOT and near the tricuspid valve during systole and diastole respectively in figure 8, consistent with the findings of Jeong *et al* (2015). Greater RV KE has been shown to be required to transport blood flow to the PA due to higher pressure there, especially in PH and repaired tetralogy of Fallot (Jeong *et al* 2015, Kamphuis *et al* 2016).

The connection between the flow patterns and quantitative metrics collected non-invasively by 4D flow MRI could also provide diagnostic potential and improvements to clinical care, particularly in the prognosis of PH (Reiter *et al* 2008, Schäfer *et al* 2017), since alterations in helical and vortical formation in the PA vasculature is known to have occurred in PH (Kamphuis *et al* 2016). The distinct differences in correlation found between enstrophy and helicity, where rotational flow is stronger in the RPA than the MPA and the LPA, would provide a quantitative basis for a more objective identification of abnormal vortices in the MPA of patients with manifest PH proposed in Reiter *et al* (2008). In addition to this, helicity and viscous energy loss have been shown in separate studies as potential haemodynamic markers of the RV function and hence prognostic markers of PH (Kamphuis *et al* 2016, Schäfer *et al* 2017). Therefore, the results of this study may lead to a better understanding of these prospective non-invasive markers of PH and the mechanisms of dissipation within the PA. Further study is needed, e.g. into the degree to which the gradient of the association between helicity and enstrophy (owing to its close relation to the dissipation) in the PA, can be used as a valid marker to indicate helical flow in patients with PH.

The characterisation of normal haemodynamic transfer of helicity density between the RV and the PA also had potential for use in patient follow-up testing in cases of repaired tetralogy of Fallot and PH where exceptional differences in helicity density have been found between volunteers and patients (Schäfer *et al* 2017, Sotelo *et al* 2018). Furthermore, the quantitative detection of flow patterns is applicable in testing the recreation of normal flow physiology and to identify optimal surgical strategies for patients with repaired tetralogy of Fallot (Geiger *et al* 2011). As in those patients, abnormal flow patterns are also typically marked by increased helical and vortical flow (Kamphuis *et al* 2016). In paediatric cardiology, in our opinion, it could also inform PA banding strategies and repair of other defects such as transposition of the great arteries and truncus arteriosus.

5. Limitations

Despite 4D flow MRI enabling versatile and comprehensive assessment of haemodynamic blood flow, limitations still exist with regard to long scan times, operator expertise and high equipment costs (van der Geest and Garg 2016). This limits the data set size in 4D flow MRI studies. The latest consensus statement paper discusses the high clinical potential of 4D flow MRI, including its application to congenital heart diseases (Isorni *et al* 2020). However, headway must still be made concerning the repeatability of the tool and testing of analysis variables for clinical utility, along with multi-centre studies to affirm the repeatability (Dyverfeldt *et al* 2015, Crandon *et al* 2017). The spatial and temporal resolutions are limited to minimise the total scan time. Interpolation scheme has been applied to enhance the resolution for PA vascular size. Interpolation may induce some overestimation in results, specifically helicity, enstrophy and dissipation rate which involve the derivative of the velocity field.

In this study, we segmented the PA vasculature at the peak systolic phase when the flow rate is maximum. The rigid PA assumption (Capuano *et al* 2019) is likely to cause an overestimation of the PA size and hence an underestimation of the density quantity in diastolic phases. However, we believe that the main results presented are not influenced significantly. This is because firstly the analyses mainly focus on the peak systolic phase, secondly the PA size during systolic phase does not change significantly (Ugander *et al* 2009). The maximum cross-sectional area change reported by Schäfer *et al* (2017) corresponds to $\approx 13.6\%$ change of equivalent diameter. Moreover, the flow quantities have very low magnitude during ventricular diastole, e.g. above 95% of the flow occurs during the systole phases, for which the segmentation is applied. No strong streamline is observed to penetrate the vessel wall, which, if occurs, is more owing to the limited spatial resolution. Recognising such limitation, streamlines which assist visualisation were mostly chosen to stem from the central area of the vessels.

6. Conclusions

In this study, we documented haemodynamic variables in the PA vasculature in structurally normal hearts, to provide additional reference to the biomedical and clinical communities to help diagnosis and development of future diagnostic tools for the right heart related abnormalities. Both flow visualisation and quantitative analyses confirmed that strong flow asymmetry is found at and near the peak systolic phases in the PA vasculature in a structurally normal heart. In particular, we noticed stronger right-handed helical flow in the RPA and weaker

Table 5. Summary of flow asymmetry quantified in the PA vasculature.

Peak stroke velocity	About 15% higher in the RPA than in the LPA; see table 1
Averaged arterial size	The RPA is larger than the LPA by 10%; see table 1
Cardiac cycle averaged bulk flow velocity	The RPA is about 40% larger than the LPA; see table 1
Correlation of the same flow quantity in different PA sections	Insignificant in general; see table 2
Correlation of different flow quantities in the same PA section	Significant in general; see table 3

left-handed helical flow in the LPA, which are linked to the positive and negative helical streams in the MPA respectively. In the MPA, flow is neither parallel nor swirls in a single direction. There appear to be two-directional helical flow winding together. The two helical streams can be of similar intensity, resulting in weak overall helicity (due to cancellation) but strong absolute helicity magnitude. The helical flow in the MPA is likely from the RV during myocardial contraction of the anisotropic RA shape. This is reflected by the strong association between the helicity density in the RV and the MPA. In terms of rotational energy, vorticity intensity in the RPA is about 20% higher than the LPA and 8% higher in the MPA. The peak sectional averaged stroke velocity as well as the averaged arterial size are also appreciably higher in the RPA than in the LAP, the ratio being 1.15 and 1.1 (diameter) respectively. The ratio of the cycle averaged bulk flow velocity in the RPA and that in the LPA is as high as 1.4. The MPA has the largest size and peak stoke velocity, as expected.

Correlations of KE and helicity between the MPA and the L/RPA sections are found to be insignificant, but the correlations of different flow quantities in the same PA vasculature are generally significant. The strong positive correlation between dissipation rate and enstrophy in both the PA and the RV is consistent with the way the dissipation is estimated given the insufficient spatial resolution. It is therefore sensible to use the enstrophy density to estimate the dissipation, which is to quantify the rate at which energy is dissipated due to small scale rotational eddies. It is plausible that the shape of the bifurcation anatomy of the PA induces flow separation and turbulence. Estimated from the KE flux, about 20% of the kinetic energy is lost from the MPA to the LPA and the RPA. Finally, the flow asymmetry quantified in this study is summarised in table 5.

Acknowledgments

This study was supported by Durham University Wolfson Research Institute Seedcorn fund; Academy of Medical Sciences start up grant with funding provided from the British Heart Foundation (SGCL7), London, United Kingdom; the Newcastle Health Care Charity and the Newcastle upon Tyne Hospitals NHS Charity (BH120740), Newcastle upon Tyne, United Kingdom. We thank all the volunteers for participating the study.

Appendix. Haemodynamic quantity calculation

The haemodynamic quantities are calculated in the same mathematical way as Dewhurst *et al* (2020), where more details can be found. For brevity, we only provide the key information here. The total volumetric kinetic energy E_k at each phase is calculated as

$$E_k = \frac{1}{2} \rho \int_V |\bar{u}|^2 dv, \quad (1)$$

where ρ is taken as 1050 kg m^{-3} for blood density and \bar{u} stands for the velocity vector. dv is the volume element and the integral volume V in this study denotes the segmented section of the RV, the MPA, the RPA or the LPA, respectively.

Vorticity, which measures the spin rate of fluid particle, is defined from velocity as $\bar{\omega} = \nabla \times \bar{u}$, where ∇ is the nabla operator. The total enstrophy is a measure of the total rotational energy in the volume, defined based on vorticity as

$$E_r = \rho \int_V |\bar{\omega}|^2 dv. \quad (2)$$

In a similar way, the total helicity is defined as

$$H = \rho \int_V (\bar{u} \cdot \bar{\omega}) dv. \quad (3)$$

Helicity intensity of a fluid particle is defined by $\bar{u} \cdot \bar{\omega}$, which is a scalar obtained by the dot product of velocity vector and vorticity vector. It measures the degree of alignment between the velocity and vorticity vectors, i.e. the

degree of the instantaneous helical motion of the local fluid particle. Unlike enstrophy and KE, helicity is not sign-definite and the polarity of helicity indicates the direction of rotation, with negative values specifying left-hand rotation and positive values right-hand rotation. Helicity is also a measure of the linkage and/or knottedness of vortex lines and hence is proportional to the cohesiveness of the flow (Schäfer *et al* 2017).

The Smagorinsky large eddy simulation method (Smagorinsky 1963) was used to give a numerical approximation of the energy dissipation rate, ϵ , and is calculated by

$$\epsilon_{ij} = -2[-(C_s \Delta)^2 S_{ij}^2] \bar{S}_{ij}, \quad (4)$$

where Δ is the length scale equivalent to the interpolated spatial resolution of 1 mm in this study. C_s is taken as an empirical constant 0.17 to work with the model and the stress tensor S_{ij} is defined by

$$\bar{S}_{ij} = \frac{1}{2} \left(\frac{\partial \bar{u}_i}{\partial x_j} + \frac{\partial \bar{u}_j}{\partial x_i} \right). \quad (5)$$

The total dissipation rate can then be calculated by

$$E_\epsilon = \rho \int_V \epsilon \, dv. \quad (6)$$

Dissipation measures the rate at which KE is dissipated to heat due to the viscous nature of the blood. Smagorinsky model is used because the current spatial resolution is not sufficient to calculate the dissipation rate directly from velocity gradient.

All of these quantities are divided by their respective volumes and thus represent densities or local intensity.

ORCID iDs

Lian Gan  <https://orcid.org/0000-0002-4948-4523>

References

- Batchelor G K 2000 *An Introduction to Fluid Dynamics* (Cambridge: Cambridge University Press)
- Bächler P, Pinochet N, Sotelo J, Crelier G, Irarrazaval P, Tejos C and Uribe S 2013 Assessment of normal flow patterns in the pulmonary circulation by using 4d magnetic resonance velocity mapping *Magn. Reson. Imaging* **31** 178–88
- Benedict R P 1980 *Fundamentals of Pipe Flow* (New York: Wiley)
- Braun F, Proença M, Lemay M, Bertschi M, Adler A, Thiran J-P and Solà J 2018 Limitations and challenges of EIT-based monitoring of stroke volume and pulmonary artery pressure *Physiol. Meas.* **39** 014003
- Capuano F, Loke Y-H and Balaras E 2019 Blood flow dynamics at the pulmonary artery bifurcation *Fluids* **4** 190
- Carlsson M, Töger J, Kanski M, Bloch K M, Ståhlberg F, Heiberg E and Arheden H 2011 Quantification and visualization of cardiovascular 4D velocity mapping accelerated with parallel imaging or k-t blast: head to head comparison and validation at 1.5 t and 3 t *J. Cardiovascular Magn. Reson.* **13** 55
- Cheng C P, Herfkens R J, Taylor C A and Feinstein J A 2005 Proximal pulmonary artery blood flow characteristics in healthy subjects measured in an upright posture using mri: the effects of exercise and age *J. Magn. Reson. Imaging* **21** 752–8
- Crandon S, Elbaz M S, Westenberg J J, van der Geest R J, Plein S and Garg P 2017 Clinical applications of intra-cardiac four-dimensional flow cardiovascular magnetic resonance: a systematic review *Int. J. Cardiol.* **249** 486–93
- Davidson P A 2015 *Turbulence: An Introduction for Scientists and Engineers* (Oxford: Oxford University Press) (<https://oxford.universitypressscholarship.com/view/10.1093/acprofoso/9780198722588.001.0001/acprof-9780198722588>)
- Dewhurst P, Coats L, Parikh J D, Hollingsworth K G and Gan L 2020 The role of flow rotation in the adult right atrium: a 4D flow cardiovascular magnetic resonance study *Physiol. Meas.* **41** 035007
- Diller G-P, Dimopoulos K, Kafka H, Ho S Y and Gatzoulis M A 2007 Model of chronic adaptation: right ventricular function in eisenmenger syndrome *Eur. Heart J. Suppl.* **9** H54–60
- Dyverfeldt P *et al* 2015 4D flow cardiovascular magnetic resonance consensus statement *J. Cardiovascular Magn. Reson.* **17** 72
- Firmin D N, Gatehouse P D, Konrad J P, Yang G Z, Kilner P J and Longmore D B 1993 Rapid 7-dimensional imaging of pulsatile flow *Proc. Computers in Cardiology Conf. (IEEE)* p 353
- Francois C, Srinivasan S, Schiebler M, Reeder S, Niespodzany E, Landgraf B, Wieben O and Frydrychowicz A 2012 4D cardiovascular magnetic resonance velocity mapping of alterations of right heart flow patterns and main pulmonary artery hemodynamics in Tetralogy of Fallot *J. Cardiovascular Magn. Reson.* **14** 16
- Gan L, Darson J R and Nickels T B 2012 On the drag of turbulent vortex rings *J. Fluid Mech.* **709** 85–105
- Geiger J, Markl M, Jung B, Grohmann J, Stiller B, Langer M and Arnold R 2011 4D-MR flow analysis in patients after repair for tetralogy of fallot *Eur. Radiol.* **21** 1651–7
- Hollingsworth K G, Blamire A M, Keavney B D and MacGowan G A 2012 Left ventricular torsion, energetics, and diastolic function in normal human aging *Am. J. Physiol.—Heart Circulatory Physiol.* **302** H885–92
- Hur D J and Sugeng L 2019 Non-invasive multimodality cardiovascular imaging of the right heart and pulmonary circulation in pulmonary hypertension *Frontiers Cardiovascular Med.* **6** 24
- Isomi M *et al* 2020 4D flow cardiac magnetic resonance in children and adults with congenital heart disease: Clinical experience in a high volume center *Int. J. Cardiol.* **320** 167–77 accepted
- Jeong D, Anagnostopoulos P V, Roldan-Alzate A, Srinivasan S, Schiebler M L, Wieben O and François C J 2015 Ventricular kinetic energy may provide a novel noninvasive way to assess ventricular performance in patients with repaired Tetralogy of Fallot *The J. Thoracic Cardiovascular Surg.* **149** 1339–47

- Jin S, Oshinski J and Giddens D P 2003 Effects of wall motion and compliance on flow patterns in the ascending aorta *J. Biomech. Eng.* **125** 347–54
- Kamphuis V, Westenberg J, Van der Palen R, Blom N, de Roos A, van der Geest R, Elbaz M S and Roest A 2016 Unravelling cardiovascular disease using four dimensional flow cardiovascular magnetic resonance *The Int. J. Cardiovascular Imaging* **33** 1069–1081
- Kheradvar A and Pedrizzetti G 2012 *Vortex Formation in the Cardiovascular System* (London: Springer)
- Kilner P J, Yang G Z, Mohiaddin R H, Firmin D N and Longmore D B 1993 Helical and retrograde secondary flow patterns in the aortic arch studied by three-directional magnetic resonance velocity mapping *Circulation* **88** 2235–47
- Kilner P, Yang G, Wilkes A, Mohiaddin R, Firmin D and Yacoub M 2000 Asymmetric redirection of flow through the heart *Nature* **404** 759–61
- Lahm T et al 2018 Assessment of right ventricular function in the research setting: knowledge gaps and pathways forward: an official American Thoracic Society research statement *Am. J. Respiratory Crit. Care Med.* **198** e15–43
- Markl M, Kilner P and Ebbers T 2011 Comprehensive 4D velocity mapping of the heart and great vessels by cardiovascular magnetic resonance *J. Cardiovascular Magn. Reson.* **13** 7
- Parikh J D, Kakarla J, Keavney B, O'Sullivan J J, Ford G A, Blamire A M, Hollingsworth K G and Coats L 2017 4D flow MRI assessment of right atrial flow patterns in the normal heart—influence of caval vein arrangement and implications for the patent foramen ovale *PLoS One* **12** 1–15
- Reiter G, Reiter U, Kovacs G, Kainz B, Schmidt K, Maier R, Olschewski H and Rienmueller R 2008 Magnetic resonance—derived 3-dimensional blood flow patterns in the main pulmonary artery as a marker of pulmonary hypertension and a measure of elevated mean pulmonary arterial pressure *Circulation: Cardiovascular Imaging* **1** 23–30
- Schäfer M, Barker A J, Kheyfets V, Stenmark K R, Crapo J, Yeager M E, Truong U, Buckner J K, Fenster B E and Hunter K S 2017 Helicity and vorticity of pulmonary arterial flow in patients with pulmonary hypertension: quantitative analysis of flow formations *J. Am. Heart Assoc.* **6** e007010
- Sharma R 2012 Pulmonary artery banding: rationale and possible indications in the current era *Ann. Pediatric Cardiol.* **5** 41–3 (PMID: 22529600)
- Smagorinsky J 1963 General circulation experiments with the primitive equations *Mon. Weather Rev.* **91** 99–164
- Sotelo J, Urbina J, Valverde I, Mura J, Tejos C, Irarrazaval P, Andia M E, Hurtado D E and Uribe S 2018 Three-dimensional quantification of vorticity and helicity from 3D Cine PC-MRI using finite-element interpolations *Magn. Reson. Med.* **79** 541–53
- Sullivan C and Trainor-Guitton W 2019 Pygeo: an open-source Python package for geoscientific visualization in vtk and paraview *J. Open Source Softw.* **4** 1451
- Sztrymf B, Souza R, Bertolotti L, Jais X, Sitbon O, Price L, Simonneau G and Humbert M 2010 Prognostic factors of acute heart failure in patients with pulmonary arterial hypertension *Eur. Respiratory J.* **35** 1286–93
- Timité B, Castelain C and Peerhossaini H 2010 Pulsatile viscous flow in a curved pipe: effects of pulsation on the development of secondary flow *Int. J. Heat Fluid Flow* **31** 879–96
- Ugander M, Jense E and Arheden H 2009 Pulmonary intravascular blood volume changes through the cardiac cycle in healthy volunteers studied by cardiovascular magnetic resonance measurements of arterial and venous flow *J. Cardiovascular Magn. Reson.* **11** 42
- van der Geest R and Garg P 2016 Advanced analysis techniques for Intra-cardiac flow evaluation from 4D flow MRI *Curr. Radiol. Rep.* **4** 38
- Vildbrad M D, Andersen A, Andersen T K, Axelgaard S, Holmboe S, Andersen S, Ringgaard S and Nielsen-Kudsk J E 2015 Limitations and pitfalls in measurements of right ventricular stroke volume in an animal model of right heart failure *Physiol. Meas.* **36** 925–37
- Wehrum T, Hagenlocher P, Lodemann T, Vach W, Dragonu I, Hennemuth A, Mühlen C, Stuplich J, Ngo B and Harloff A 2016 Age dependence of pulmonary artery blood flow measured by 4D flow cardiovascular magnetic resonance: results of a population-based study *J. Cardiovascular Magn. Reson.* **18** 31